Generalized Topologies of Single-Stage Input-Current-Shaping Circuits

Laszlo Huber[1], Jindong Zhang[2], Milan M. Jovanoviæ[1], and Fred C. Lee[2]

[1] Delta Products Corporation
Power Electronics Laboratory
P.O. Box 12173
5101 Davis Drive
Research Triangle Park, NC 27709

[2] Center for Power Electronics Systems
The Bradley Department of Electrical Engineering
Virginia Polytechnic Institute and State University
Blacksburg, VA 24060 – 0111

Abstract - In this paper, two generalized topologies of single-stage input current shaping (S^2ICS) circuits are derived: S^2ICS circuits with two-terminal ICS cells and S^2ICS circuits with three-terminal ICS cells. It is shown that most of the recently published S^2ICS circuits belong to either of the two generalized topologies. It is also shown that the two generalized S^2ICS topologies are functionally equivalent. Based on the generalized approach, a few new S^2ICS circuits are developed. Experimental results obtained on a selected pair of S^2ICS circuits with 2-terminal and 3-terminal ICS cells are also provided.

I. INTRODUCTION

A number of single-stage input current shaping (S^2ICS) converters have been introduced recently [1-10]. Unlike the two-stage converters with input current shaping (ICS), in a S^2ICS converter, the ICS switch and its controller are saved and ICS, isolation, and high-bandwidth output-voltage control are performed in a single conversion step, i.e., without creating a regulated dc bus. All these S^2ICS circuits integrate a boost ICS stage with a forward or flyback dc/dc-converter stage. The ICS inductor of a S^2ICS circuit can operate either in the discontinuous conduction mode (DCM) or in the continuous conduction mode (CCM). In the DCM operation of the ICS inductor, low line-current harmonic distortions are achieved because of the inherent property of the DCM boost converter to draw a near sinusoidal current if its duty cycle is held relatively constant during a half line cycle. The implementation of the CCM operation of the ICS inductor is more challenging because a single switch has to control two different duty cycles; i.e., a constant duty cycle of the dc/dc converter (in steady state) and a variable duty cycle of the ICS inductor. Usually, the DCM operation gives a lower total harmonic distortion (THD) of the line current compared to the CCM operation. However, the CCM operation yields a slightly higher efficiency compared to the DCM operation. A detailed review of the S^2ICS converters is presented in [11].

Generally, S^2ICS converters meet European and/or Japanese regulatory requirements regarding line current harmonics, but they do not improve the power factor (PF) and reduce the THD as much as their conventional two-stage counterparts. Typically, PF for the S^2ICS converters is between 0.8 and 0.9, whereas their THD is in the 40-75% range.

In order to better understand the differences and similarities between different S^2ICS circuits as well as to develop new S^2ICS topologies, a generalization of the S^2ICS circuits is performed in this paper. It is shown that most of the recently published S^2ICS circuits can be classified in two families: the S^2ICS family with 3-terminal ICS cells and the S^2ICS family with 2-terminal ICS cells. It is shown that, although topologically different, the two S^2ICS families are functionally equivalent and exhibit very similar performance. Advantages and disadvantages of the two S^2ICS families are discussed. Using the generalized approach, a few new S^2ICS circuits are developed. Finally, experimental results obtained on a selected pair of S^2ICS circuits with 2-terminal and 3-terminal ICS cells are provided.

II. GENERALIZED S^2ICS TOPOLOGIES

A. S^2ICS Family with 3-Teminal ICS Cells

A typical S^2ICS circuit with DCM operation of the ICS inductor is shown in Fig. 1 [4]. In this circuit, a boost ICS stage and a flyback or forward dc/dc converter stage are combined into a single stage. The ICS cell, shown in the dotted rectangle in Fig. 1, includes boost inductor L_B and two current paths: path XZ for charging L_B when switch S is on and path XY for discharging L_B when switch S is off. Since charging path XZ is connected to switch S and discharging path XY is connected to bulk capacitor C_B, the ICS cell in

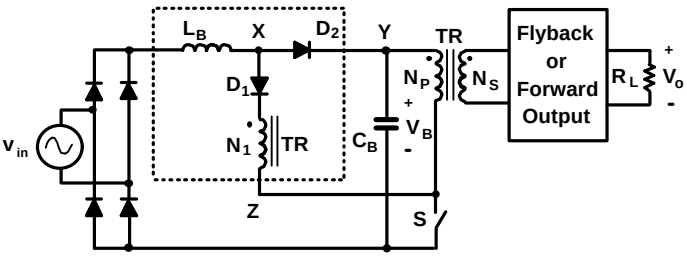

Fig. 1 DCM S^2ICS circuit with additional winding N_1 [4]

This work was supported in part by a fellowship from Delta Electronics, Inc., Taiwan.
Besides, This work made use of ERC Shared Facilities supported by the U.S. National Science Foundation under Award Number EEC-9731677

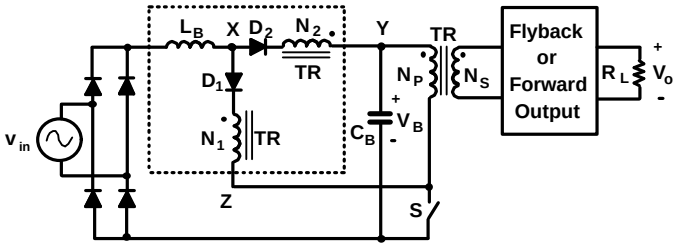

Fig. 2 DCM S^{2}ICS circuit with additional windings N_1 and N_2 [5]

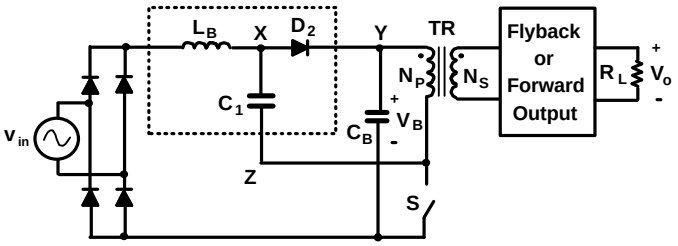

Fig. 4 S^{2}ICS circuit with 3-terminal capacitive CCM-ICS cell [1]

Fig. 1 has three terminals. The function of the transformer winding N_1 is to limit the voltage on bulk capacitor C_B and to improve the overall efficiency. In fact, when switch S is closed, the induced voltage across winding N_1 is in opposition to the rectified line voltage; as a result, to keep the same volt-second product across L_B, a larger duty cycle is necessary. With a larger duty cycle and the inductor of the dc/dc power stage operating in CCM, the bulk-capacitor voltage is reduced. However, winding N_1 also introduces line-current distortions around the zero crossings because the line current cannot flow when the instantaneous line voltage is lower than the voltage induced across winding N_1. Therefore, in the S^{2}ICS circuit in Fig. 1 there is a strong trade-off between PF, THD, and efficiency. To further reduce the bulk capacitor voltage and improve efficiency, another transformer winding, N_2, can be placed in discharging path XY [5] as shown in Fig. 2. During the discharging of the ICS inductor, the voltage across windings N_2 has the same direction as the voltage across the bulk capacitor, i.e., winding N_2 effectively increases the reset voltage across the ICS inductor. As a result, the required reset voltage for L_B can be obtained with a lower voltage on bulk capacitor C_B. It should be noted that since windings N_1 and N_2 are magnetically coupled to the secondary winding of transformer TR, they can be used to directly transfer energy from the input (line) to the load. Winding N_1 provides direct energy transfer with the forward-type dc/dc power stages, while winding N_2 provides direct energy transfer with the flyback-type dc/dc power stages. Generally, direct energy transfer improves the conversion efficiency.

To achieve CCM operation of the ICS inductor, an additional inductor or capacitor is required as shown in Figs. 3 [6], [8], [9] and 4 [1], respectively. The function of inductor L_1 in Fig. 3 and capacitor C_1 in Fig 4 is to provide a variable effective duty cycle for boost inductor L_B even when the duty cycle of switch S is relatively constant during a half line cycle. Namely, to achieve a good tracking of the line current and line voltage with boost inductor L_B operating in CCM, it is necessary that the duty cycle of L_B, D_{LB}, defined as the ratio of the charging time of L_B and the switching period, is proportional to the instantaneous line voltage during a half line cycle. Specifically, D_{LB} should be maximum around the zero crossings of the line voltage and minimum around the line voltage peaks, i.e.,

$$D_{LB} \approx 1 - |v_{in}| / V_B \ . \qquad (1)$$

Inductor L_1 in Fig. 3 modulates boost-inductor duty cycle D_{LB} by delaying the commutation of the boost inductor current from path XY to path XZ after switch S is turned on. Since during this commutation time, which is proportional to the line current and, therefore, to the line voltage, L_B continues to discharge, duty cycle D_{LB} varies with the line voltage even though the duty cycle of switch S is relatively constant. Similarly, in Fig. 4, capacitor C_1 modulates D_{LB} by speeding up the commutation of the boost-inductor current from path XZ to path XY after switch S is turned on. Namely, after switch S is turned on, boost-inductor current charges capacitor C_1 until C_1 is charged to V_B. Once C_1 is charged to V_B, the boost-inductor current commutates to path XY. As a result, duty cycle D_{LB} is different from the duty cycle of switch S. Furthermore, since the charging time of C_1 is proportional to the boost-inductor current, D_{LB} varies with the line voltage as shown in (1).

In all S^{2}ICS circuits in Figs. 1-4, the 3-terminal ICS cell, shown in the dotted rectangle, has the same basic topology

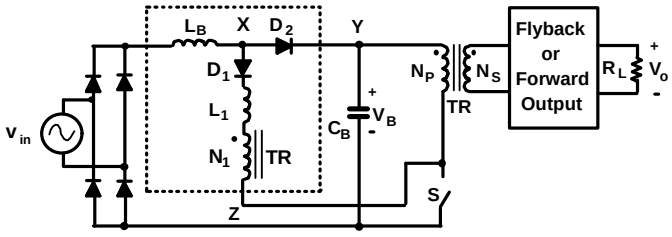

Fig. 3 S^{2}ICS circuit with 3-terminal inductive CCM-ICS cell [6], [8], [9]

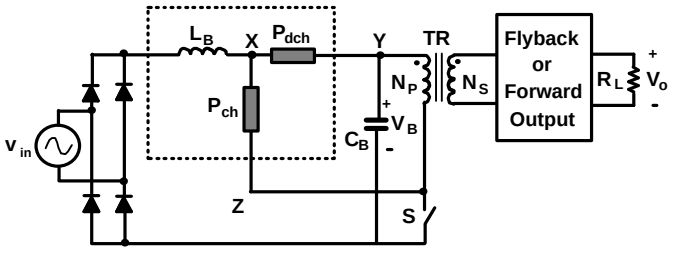

Fig. 5 Generalized topology of S^{2}ICS circuit with 3-terminal ICS cell

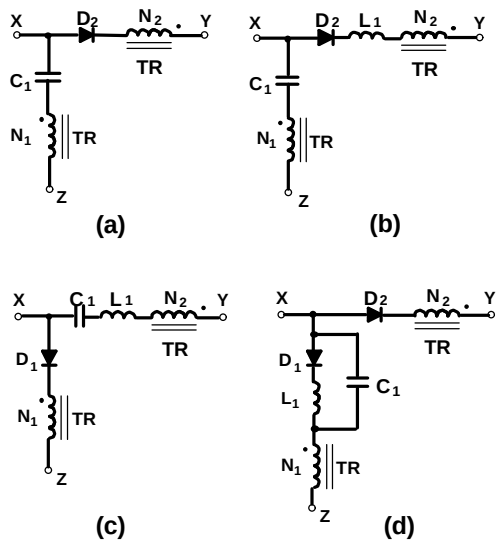

Fig. 6 New implementations of 3-terminal ICS cells (ICS inductor is not shown)

that includes ICS inductor L_B connected to the output of the full-bridge rectifier, L_B charging path XZ connected to switch S, and L_B discharging path XY connected to bulk capacitor C_B. Therefore, all S^{2}ICS circuits in Figs. 1-4 can be represented by a S^{2}ICS circuit with a generalized 3-terminal ICS cell as shown in Fig. 5. The generalized 3-terminal ICS cell in Fig. 5 consists of ICS inductor L_B, the boost inductor charging path P_{ch} between nodes X and Z, and the boost inductor discharging path P_{dch} between nodes X and Y. The L_B charging and discharging paths each includes at least one of the following components: a diode, a transformer winding, an inductor, and a capacitor.

Using this generalized approach, it can be concluded that the charging and discharging paths of the boost inductor can be implemented with many different combinations of diodes, inductors, capacitors, and additional windings of the transformer in the dc/dc power stage. A number of possible new implementations of the 3-terminal ICS cells are shown in Fig. 6. It should be noted that in all implementations of the 3-terminal ICS cell in Fig. 6, boost inductor L_B operates in the CCM: CCM operation of L_B is achieved by additional capacitor C_1 in Fig. 6(a), and by both additional inductor and capacitor in Figs. 6(b)-6(d).

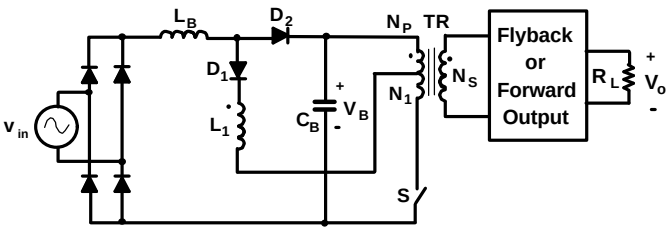

Fig. 7 Implementation of winding N_1 in the 3-terminal ICS cell in Fig. 3 by tapping the primary winding of the power transformer

Finally, it should be noted that windings N_1 and N_2 in Figs. 1-6 can be implemented by tapping the primary winding of the power transformer [8], [9], [10]. As an example, Fig. 7 shows the implementation of winding N_1 in the 3-terminal ICS cell in Fig. 3 as a portion of the primary winding of transformer *TR*. While tapping simplifies the transformer design, it has no effect on the operation of the S^{2}ICS circuits.

B. S^{2}ICS Family with 2-Teminal ICS Cells

Another implementation of the DCM S^{2}ICS circuit is shown in Fig. 8 [3]. The S^{2}ICS circuit in Fig. 8 can be redrawn as shown in Fig. 9. In this implementation, a 2-terminal ICS cell, shown in the dotted rectangle, is inserted between the full-bridge rectifier and the bulk capacitor. The 2-terminal ICS cell in Fig. 9 consists of ICS inductor L_B, the charging path of L_B (the path with D_1 and N_1^*), and the discharging path of L_B (the path with D_2). The charging and discharging paths of L_B are connected in parallel. The polarity of transformer winding N_1^* is such that the voltage across it is in opposition to the bulk voltage V_B during the on-time of switch S, therefore, decreasing the voltage at node X. To obtain the same voltage at node X during the on-time of switch S as in the corresponding 3-terminal cell in Fig. 1, the number of turns of winding N_1^* should be

$$N_1^* = N_P - N_1 \quad , \tag{2}$$

where N_1 is the number of turns of winding N_1 in Fig. 1. The discharging path of L_B in the 2-terminal ICS cell in Fig. 9 is identical to the discharging path of L_B in the corresponding 3-

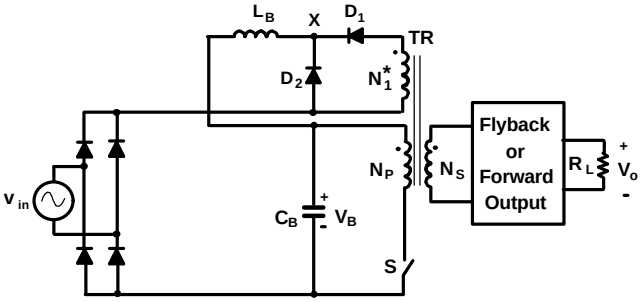

Fig. 8 DCM S^{2}ICS circuit with 2-terminal ICS cell [3]

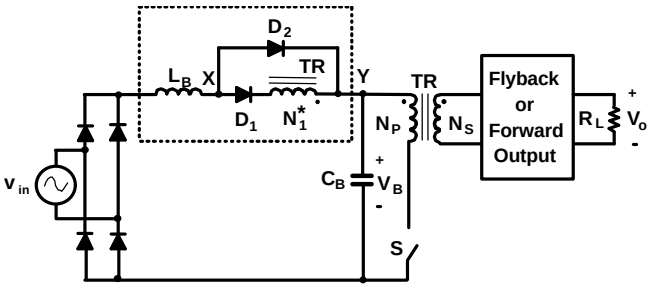

Fig. 9 DCM S^{2}ICS circuit with 2-terminal ICS cell in Fig. 8 redrawn

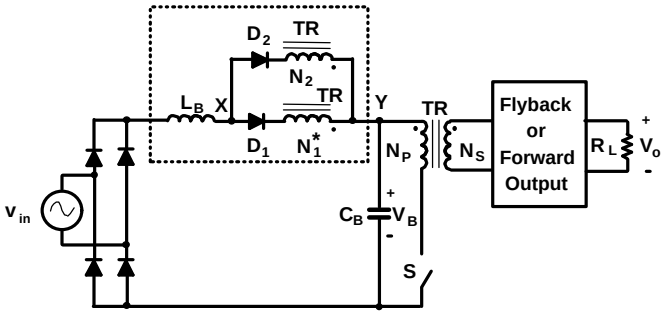

Fig. 10 DCM S^2ICS circuit with 2-terminal ICS cell corresponding to DCM S^2ICS circuit with 3-terminal ICS cell Fig. 2

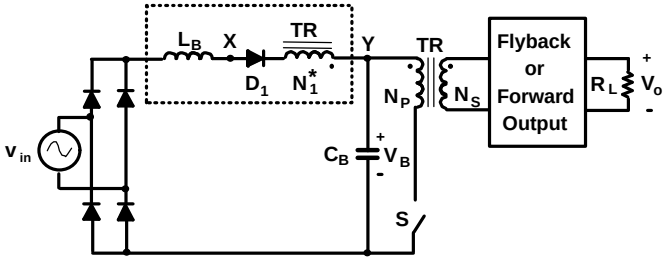

Fig. 11 DCM S^2ICS circuit with 2-terminal ICS cell (Magnetic switch power supply) [2]

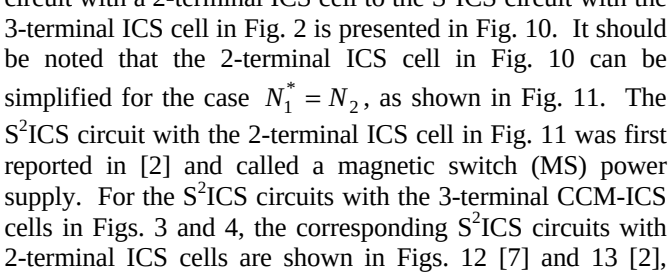

Fig. 12 S^2ICS circuit with 2-terminal inductive CCM-ICS cell [7]

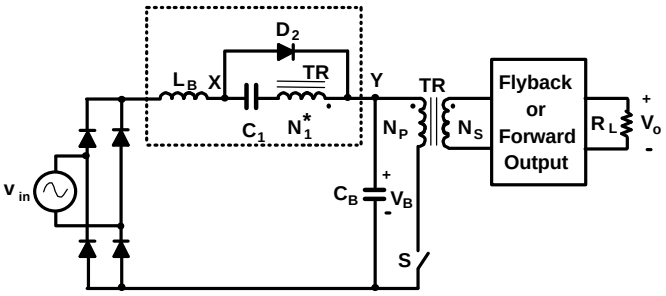

Fig. 13 S^2ICS circuit with 2-terminal capacitive CCM-ICS cell [2]

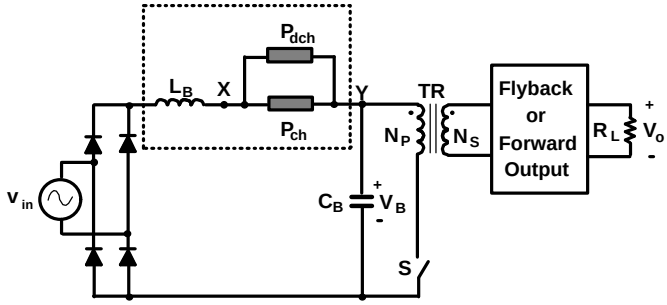

Fig. 14 Generalized topology of S^2ICS circuit with 2-terminal ICS cell

terminal ICS cell in Fig. 1. Therefore, with $N_1^* = N_P - N_1$, the S^2ICS circuit with the 2-terminal ICS cell in Fig. 9 is functionally equivalent to the S^2ICS circuit with the 3-terminal ICS cell in Fig. 1.

Generally, for each S^2ICS circuit with a 3-terminal ICS cell in Figs. 1-6, there exists a functionally equivalent S^2ICS circuit with a 2-terminal ICS cell. The corresponding S^2ICS circuit with a 2-terminal ICS cell to the S^2ICS circuit with the 3-terminal ICS cell in Fig. 2 is presented in Fig. 10. It should be noted that the 2-terminal ICS cell in Fig. 10 can be simplified for the case $N_1^* = N_2$, as shown in Fig. 11. The S^2ICS circuit with the 2-terminal ICS cell in Fig. 11 was first reported in [2] and called a magnetic switch (MS) power supply. For the S^2ICS circuits with the 3-terminal CCM-ICS cells in Figs. 3 and 4, the corresponding S^2ICS circuits with 2-terminal ICS cells are shown in Figs. 12 [7] and 13 [2], respectively. The S^2ICS circuit with the generalized 2-terminal ICS cell is shown in Fig. 14. Finally, possible new implementations of the 2-terminal ICS cells, which correspond to the new implementations of the 3-terminal ICS cells in Fig 6, are shown in Fig. 15.

Generally, the S^2ICS circuits with 2-terminal and 3-terminal ICS cells are functionally equivalent and, hence, they exhibit similar performance. Differences between them

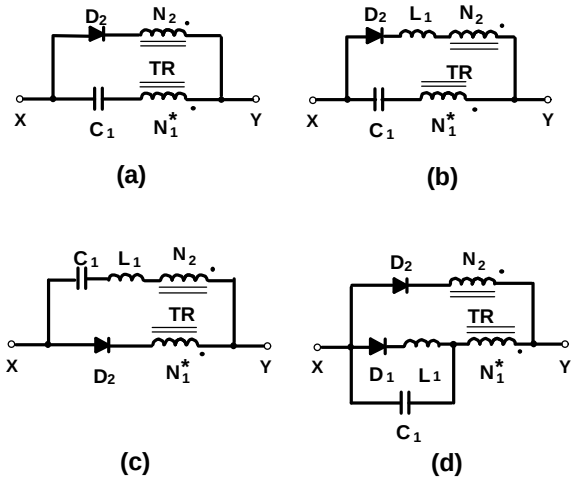

Fig. 15 New implementations of 2-terminal ICS cells (ICS inductor is not shown)

are mostly related to the transformer design. A S^{2}ICS circuit with a 2-terminal ICS cell requires at least one additional transformer winding (winding N_1^* in Figs. 8-15) and, consequently, it may require a larger transformer than the corresponding S^{2}ICS circuit with a 3-terminal ICS cell if winding N_1 is implemented by tapping the primary winding of the transformer. It should be noted that the S^{2}ICS circuits with 3-terminal ICS cells are limited to single-ended topologies such as the single-switch forward and flyback converters. On the other hand, the S^{2}ICS circuits with 2-terminal ICS cells can be implemented with any isolated dc/dc converter such as the 2-switch and the full-bridge forward converters.

III. Experimental Results

To experimentally verify the conclusions in Section II, a pair of S^{2}ICS circuits with 3-terminal and 2-terminal inductive CCM-ICS cells shown in Figs. 7 and 12, respectively, with a forward output was selected. The experimental S^{2}ICS circuits were designed for a 200-W (5-V/40-A), 180–265-V_{rms} line-voltage power supply. The major components of the circuit are as follows: L_B = 408 µH, L_1 = 124 µH, TR – EER35 core with N_P = 49 turns, N_S = 3 turns, N_1 = 25 turns, N_1^* = 24 turns, C_B – 220 µF/

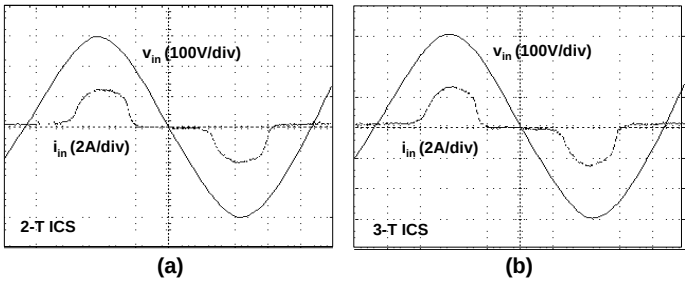

Fig. 16 Experimental line-voltage and line-current waveforms of the S^{2}ICS circuit with (a) 2-terminal and (b) 3-terminal ICS cell at nominal line (V_{in} = 230 V_{rms}) and full load (I_o = 40 A)

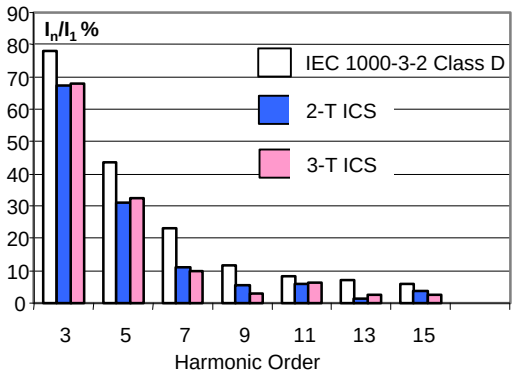

Fig. 17 Experimental line-current harmonics at nominal line (V_{in} = 230 V_{rms}) and full load (I_o = 40 A)

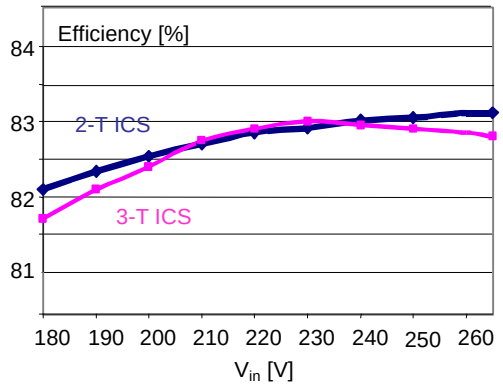

Fig. 18 Efficiency measurements versus line voltage at full load

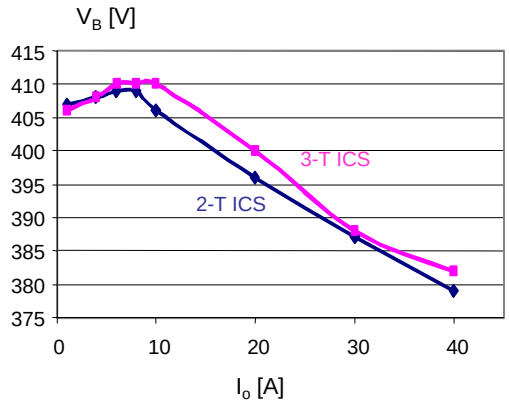

Fig. 19 Bulk-voltage measurements versus load current at maximum line voltage (V_{in} = 265 V_{rms})

450 V, S - IXFH12N100, and secondary-side diodes - 81CNQ045. The reset of the forward transformer was achieved with a reset winding. The switching frequency was 70 kHz. The control circuit was implemented using the low-cost integrated controller UC3825A.

Measured line-voltage and line-current waveforms at nominal line (V_{in} = 230V_{rms}) and full load (I_o = 40A) for both implementations are shown in Fig. 16. As can be seen, the line-current waveforms are almost identical. The corresponding line-current harmonics are shown in Fig. 17. The harmonic limits for the IEC 1000-3-2 Class D standard are also given in Fig. 17. Both implementations satisfy the IEC 1000-3-2 Class D standard with enough margins. Comparative efficiency measurements at full load versus line voltage are presented in Fig. 18. The difference between the efficiencies of the two implementations is less than 0.5%. Finally, comparative bulk-voltage measurements at maximum line voltage (V_{in} = 265V_{rms}) versus load current are presented in Fig. 19. For both implementations, the maximum bulk voltage is around 410 V which was obtained at a load current slightly below 10 A.

All the experimental results in Figs. 16-19 verify that the two implementations of the selected S^2ICS circuit with 3-terminal and 2-terminal inductive CCM-ICS cells exhibit only minor performance differences, which is the result of the slightly different transformer structure and, eventually, the measurement error.

IV. SUMMARY

Two generalized topologies of single-stage input-current-shaping (S^2ICS) circuits are presented: S^2ICS circuits with 2-terminal ICS cells and S^2ICS circuits with 3-terminal ICS cells. It was shown analytically and verified experimentally that the two generalized S^2ICS topologies are functionally equivalent.

REFERENCES

[1] S. Teramoto, M. Sekine, and R. Saito, "High power factor ac/dc converter," U.S. Patent No. 5,301,095, Apr. 5, 1994.

[2] H. Watanabe, Y. Kobayashi, Y. Sekine, M. Morikawa, and T. Ishii, "The suppressing harmonic currents, MS (magnetic-switch) power supply," *IEEE International Telecommunications Energy Conf. (INTELEC) Proc.*, pp. 783-790, Oct. 1995.

[3] M. Daniele, P. Jain, and G. Joos, "A single stage single switch power factor corrected ac/dc converter", *IEEE Power Electronics Specialist Conf. (PESC) Rec.*, pp. 216-222, Jun. 1996.

[4] F.S. Tsai, P. Markowski, and E. Whitcomb, "Off-line flyback converter with input harmonic current correction," *IEEE International Telecommunication Energy Conf. (INTELEC) Proc.*, pp. 120-124, Oct. 1996.

[5] L. Huber and M.M. Jovanoviæ, "Single-stage, single-switch, isolated power supply technique with input-current-shaping and fast output-voltage regulation for universal input-voltage-range applications," *IEEE Applied Power Electronics Conf. (APEC) Proc.*, pp. 272-280, Feb. 1997.

[6] L. Huber and M.M. Jovanoviæ, "Design optimization of single-stage, single-switch input-current shapers," *IEEE Power Electronics Specialist Conf. (PESC) Rec.*, pp. 519-526, Jun. 1997.

[7] J. Sebastian, M.M. Hernando, P. Villegas, J. Diaz, and A. Fontan, "Input current shaper based on the series connection of a voltage source and a loss-free resistor," *IEEE Applied Power Electronics Conf. (APEC) Proc.*, pp. 461-467, Feb. 1998.

[8] J. Sebastian, M.M. Hernando, P. Villegas, J. Diaz, and A. Fontan, "A new input current shaping technique using converters operating in continuous conduction mode," *IEEE Power Electronics Specialist Conf. (PESC) Rec.*, pp. 1330-1336, May 1998.

[9] G. C. Hua, "Consolidated soft-switching ac/dc converters," U.S. Patent No. 5,790,389, Aug. 4, 1998.

[10] L. Huber and M.M. Jovanoviæ, "Single-stage, single-switch input-current-shaping technique with reduced switching loss," *IEEE Applied Power Electronics Conf. (APEC) Proc.*, pp. 98-104, Mar. 1999.

[11] C. Qian and K.M. Smedley, "A topology survey of single-stage power factor corrector with a boost type input-current shaper," *IEEE Applied Power Electronics Conf. (APEC) Proc.*, pp. 460-467, Feb. 2000.